Sound generation in coflow and counterflow mixing layers

Ge Song, Xavier Gloerfelt, Jean-Christophe Robinet

10ème **C**ongrès **F**rançais d'**A**coustique

Lyon, 12-16 Avril 2010

Sound generation in coflow and counterflow mixing layers

Ge Song[1], Xavier Gloerfelt[1], Jean-Christophe Robinet[1]

[1] Laboratoire DYNFLUID, Arts & Métiers ParisTech, 151 Bd. de l'Hôpital, 75013 Paris, ge.song@ensam.eu

In this study, nonlinear disturbance equations are solved in two and three dimensions to investigate the sound generated by compressible plane mixing layers. Two flow regimes are distinguished : coflow and counterflow mixing layers. The simulations of coflow shear layers has been carried out in two- and three-dimensions. In both cases, the main radiation is attributed to the pairing events leading to a quadrupolar signature. The convective nature of the flow is conform with the linear stability calculations. On the contrary, the two-dimensional simulation of a counterflow mixing layer illustrates a typical oscillator behaviour of the flow.

1 Introduction

The goal of computational aeroacoustics (CAA) is the calculation of the acoustic fluctuations generated by fluid flows to study the noise generation mechanisms. Compared to traditional CFD techniques, some critical issues that are typical of CAA need to be addressed : the nondispersive and nondissipative character of acoustic waves ; the extremely low amplitude of acoustic perturbations compared to mean flow values ; and the high frequencies of waves that need to be solved. Among the current CAA methods, Direct Numerical Computations (DNC) have been largely used. In this direct approach, neither modeling nor simplifying assumptions are used, the compressible unsteady equations of flow motion are solved to simulate both aerodynamic and acoustic fields. This kind of approaches is well suited to investigate the link between the acoustic emissions and the coherent vortical structures. The dynamics of these coherent motions can be predicted by the linear stability theory. The aim of the present work is thus to study the noise radiations associated with the instability waves in the canonical free shear layer flows. Several previous numerical studies are relevant to the present topic. For instance, the temporal simulations of Comte *et al.* [1] have displayed the evidence for helical pairing, where vortex filaments ocillate out-of-phase in the spanwise direction, and reconnect, yielding a vortex-lattice structure. Colonius *et al.* [2], as well as Bogey *et al.* [3] have used a 2D DNC to investigate the sound generated by vortex pairing in a plane coflow mixing layer. Recently, Babuke *et al.* have performed two- and three-dimensional DNC to simulate the noise generation mechanism in a compressible coflow mixing layer. In their study, they predicted a tonal noise source in two-dimensions whereas broad band noise was emitted in three-dimensional simulation. Also, some previous theoretical studies indicated the role of the instability waves in aeroacoustics of jets and mixing layers (Tam & Morris [5] and Tam & Burton [6], [7]). To date, few three-dimensional simulations have been performed to study the sound generation mechanism of a coflow mixing layer. And, a comprehensive study has not yet been undertaken to examine the near-field aerodynamics or the radiated acoustic field in a counterflow mixing layer.

The rest of the paper is organized as follows. First, the governing equations are presented. Next, the numerical algorithm is explained, along with the boundary conditions treatments. Then, the shear layer dynamics, the combined stability calculations and some acoustic characteristics of a two-dimensional coflow and counterflow mixing layers are contrasted and compared. Finally, the three-dimensional simulation results of a coflow mixing layer is presented.

2 Governing equations

In this paper, we apply a CAA methodology, proposed by Morris *et al.* [8], to compute the noise radiation. The method splits the instantaneous physical variables of the flow into a mean flow and a perturbation. In the present investigation, any given base flow is by construction a steady state solution of the governing equations, thus a base flow is chosen instead of a mean flow. The governing equations for the perturbations, called here the nonlinear disturbance equations (NLDE), consist of linear and nonlinear fluctuation terms, and a base flow source term that is independent of the fluctuations. The acoustic and perturbation quantities are obtained directly by using this methodology. As we calculate only the acoustic and aerodynamic perturbations, this makes the boundary conditions treatment easier.

The nonlinear disturbance equations (NLDE) are obtained from the conventional Reynolds decomposition of the Euler equations. Noting $\mathcal{E}$ the corresponding Euler equations operator, this yields.

$$\mathcal{E}(\bar{U} + U') = 0 \tag{1}$$

and

$$\mathcal{E}(\bar{U}) = 0 \tag{2}$$

Substitution of (1) into (2) results in a set of perturbation fluxes and base flow flux terms in a non-conservative form, as :

$$\frac{\partial U'}{\partial t} + \frac{\partial E'}{\partial x} + \frac{\partial F'}{\partial y} + \frac{\partial G'}{\partial z} + H' = 0, \tag{3}$$

with

$$U' = \begin{pmatrix} \rho' \\ \rho u' \\ \rho v' \\ \rho w' \\ p' \end{pmatrix}$$

where the convective fluxes are given by

$$E' = \begin{pmatrix} \rho u' + \rho' \bar{u} \\ \rho u v + p' \\ \rho u v' \\ \rho u w' \\ p' \bar{u} + \gamma p u' \end{pmatrix} \quad F' = \begin{pmatrix} \rho v' + \rho' \bar{v} \\ \rho v u' \\ \rho v v' + p' \\ \rho v w' \\ p' \bar{v} + \gamma p v' \end{pmatrix}$$

$$G' = \begin{pmatrix} \rho w' + \rho' \bar{w} \\ \rho w u' \\ \rho w v' \\ \rho w w' + p' \\ p' \bar{w} + \gamma p w' \end{pmatrix}$$

$$H' = \begin{pmatrix} 0 \\ H_1 \\ H_2 \\ H_3 \\ (\gamma - 1)(p' \nabla \bar{\mathbf{u}} - u' \dfrac{\partial p}{\partial x} - v' \dfrac{\partial p}{\partial y} - w' \dfrac{\partial p}{\partial z}) \end{pmatrix}.$$

where

$$H_j = \sum_{i=1}^{3} \frac{\partial \bar{u_j}}{\partial x_i} (\rho u_i' + \rho' \bar{u_i})$$

In these equations, ρ', p', u', v' and w' are the perturbation density, pressure and velocity components, while their base flow counterparts are $\bar{\rho}$, $\bar{p}$, $\bar{u}$, $\bar{v}$ and $\bar{w}$. The ratio of specific heats γ is set to 1.4.

3 Numerical features

The discretized equations are advanced in time using an optimized fourth-order Runge-Kutta scheme. The spatial derivatives are calculated using a fourth-order optimized dispersion relation preserving (DRP) scheme of Tam & Webb [9]. An eleven-point stencil is used for the DRP scheme in the present work. Following Bogey & Bailly [10], an eleven-point stencil selective filter is added to damp out spurious short waves. Tam & Dong [11] radiation boundary conditions are used at the far-field boudaries and outflow conditions are imposed at the downstream boundary. A combination of grid stretching in the streamwise direction and Laplacian filtering is employed in the sponge region to reduce the amplitude of flow perturbations before they interact with the downstream boundary, thus diminishing the acoustic reflections.

4 Flow configuration

We consider a mixing layer periodic in the spanwise direction, initiated by a hyperbolic-tangent velocity profile, as shown in Figure 1.

$$\bar{u}(y) = \frac{U_1 + U_2}{2} + \frac{U_1 - U_2}{2} \tanh\left(\frac{2y}{\delta_\omega(0)}\right) \qquad (4)$$

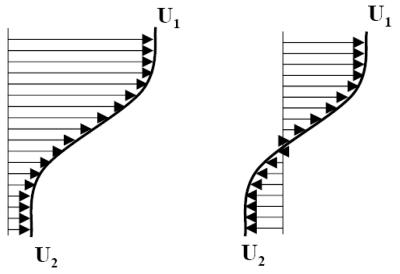

FIG. 1: Coflow and counterflow mixing layer configuration

The velocities of the upper and lower streams are U_1 and U_2. The vorticity thickness is the distance defined by the ratio of the velocity difference across the layer $\Delta U = U_1 - U_2$ divided by the maximum slope of the velocity profile

$$\delta_\omega(x) = \frac{\Delta U}{|(\partial \bar{u}/\partial y)|_{max}} \qquad (5)$$

with $\delta_\omega(0)$ the initial vorticity thickness. As only relative motions are important, the Mach number used to characterize compressibility effects must be based on the difference between the convective speed of the large eddies and the velocities of the external flows. In our case, the two external flows have the same γ, and the evolution is isentropic. Thus, a simplier expression is obtained : $M_c = (U_1 - U_2)/2c_0$. According to the criterion developed in the study of free shear flow instabilities by Huerre & Monkewitz [12], a mixing layer is convectively unstable when the velocity ratio $R = \Delta U/2\bar{U}$ is smaller than $R_t = 1.315$ where $\bar{U}$ their average velocity. Otherwise the mixing layer is considered to be absolutely unstable. We indeed distinguish two main classes of instabilities : selective noise amplifiers which are very sensitive to external forcing, and oscillators, which resonate at a specific intrinsic frequency. Here, coflow mixing layers display amplifier-type behavior whereas counterflow mixing layers behave like oscillators.

5 Two-dimensional mixing layers

5.1 Coflow mixing layer

5.1.1 Numerical parameters

The aim is to investigate the sound generation by excited mixing layers. The base flow corresponds to equation (4) with a high-speed stream at 160 m/s and a low-speed stream at 40 m/s. The initial vorticity thickness is $\delta_\omega(0) = 0.0016$ m. The temperatures of the two free streams are equal. The computational domain extends over $x = 200\delta_\omega(0)$ in the streamwise direction and from $y = -300\delta_\omega(0)$ to $y = 300\delta_\omega(0)$ in the cross-flow direction. It is discretized by a Cartesian grid of 440 by 440 grid points, which is uniform over the first 340 points with spacing $\Delta x = 0.32\delta_\omega(0)$, and then stretched over the last 100 points. The Laplacian sponge zone is progressively applied from $x = 170\delta_\omega(0)$. In the transverse direction, the mesh size is $\Delta y = 0.16\delta_\omega(0)$ inside the shear layer, and reaches a value $\Delta y = 3\delta_\omega(0)$ in the far-field. A CFL number of 1 is used.

5.1.2 Inflow forcing

The mixing layer is forced near the inlet plane by a combination of two waves at the fundamental frequency f_0 and its subharmonic $f_0/2$, where f_0 denotes the frequency of the most unstable instability wave. The frequencies of these waves are determined by linear stability analysis of the corresponding inviscid parallel flow. The forcing is applied on the normal velocity component :

$$v'(y) = (\alpha_1 \sin \omega t + \alpha_2 \sin(\frac{\omega}{2}t + \frac{\pi}{2})) \exp\left(-\frac{y^2}{\Delta y^2}\right) \quad (6)$$

where the pulsation ω is given by $\omega = 2\pi f_0$. The transverse distribution of the excitation follows a Gaussian distribution centered at the shear layer location. The amplitudes of the two frequencies are $\alpha_1 = 2.10^{-4}$ and $\alpha_2 = 10^{-4}$ m/s. The particular excitation combining f_0 and $f_0/2$ aims at fixing the location of the first vortex pairing.

5.1.3 Linear stability calculation

Within the convective instability framework, spatial amplification rate versus pulsation ω for the given hyperbolic-tangent velocity profile is sketched in figure 2. The fundamental frequency is found at the maximum amplification rate, in our case, $f_0 = \bar{U}\omega/2\pi\delta_\omega(0) = 8166$ Hz.

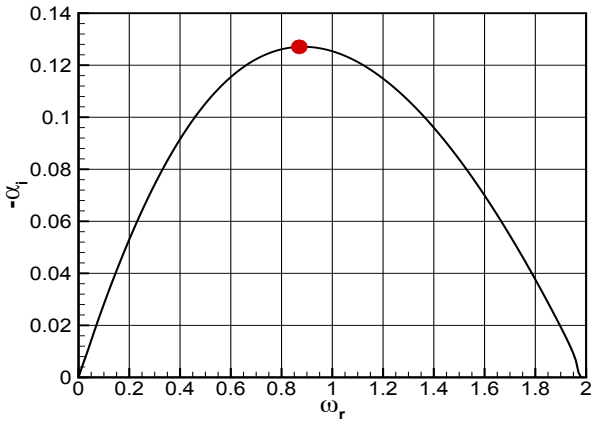

FIG. 2: Spatial amplification rate versus pulsation of the coflow mixing layer.

5.1.4 Near-field hydrodynamic results

We present the results in two parts : a near-field region, where the aerodynamic motions are dominant, and a far-field region, where the acoustic behaviour is represented. In the vorticity view of figure 3, the roll up of well-defined Kelvin-Helmholtz vortices are visible after several oscillations. A train of vortices is then shed at the fundamental frequency. Vortex pairing processes are shown at a fixed location around $x = 70\delta_\omega(0)$, due to the particular inflow forcing. Afterwards, the shedding frequency is $f_0/2$, associated with the doubling of spanwise rolls. We can note that the vortices are dissipated as they enter the sponge zone.

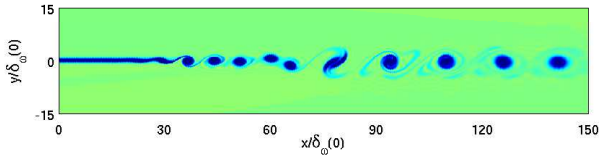

FIG. 3: Total vorticity field of the two-dimensional coflow mixing layer excited by the fundamental frequency f_0 the first subharmonic $f_0/2$. Levels from -5×10^4 to $5 \times 10^4 \mathrm{s}^{-1}$.

5.1.5 Acoustic radiation

Figure 4 clearly shows wavefronts emanating from the vortex pairing location. Furthermore, the frequency of acoustic waves is $f_p = f_0/2 = 4083$ Hz, confirming that acoustic waves are generated by the pairing events. The acoustic near-field is characteristic of a lateral quadrupolar source. The wave fronts are affected by convection effects, especially in the high-speed zone where the Doppler effect is more marked, changing the main direction of the upper radiation lobe. It can be noted that the radiation is more pronounced in the downstream direction as observed in the work of Colonius *et al.* [2].

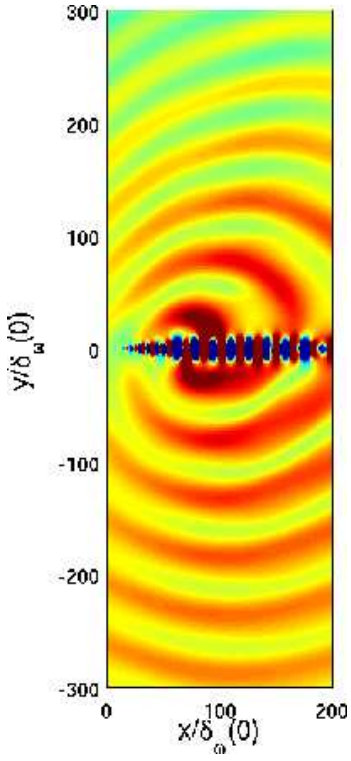

FIG. 4: Far-field pressure for a coflow mixing layer forced at f_0 and $f_0/2$. Pressure levels from -150 Pa to 150 Pa.

5.2 Counterflow mixing layer

5.2.1 Numerical parameters

The velocities of the upper and lower streams are $U_1 = 160$ m/s and $U_2 = -40$ m/s, yielding a convective Mach number is $M_c = 0.29$. The velocity ratio is $R = 1.67$ in this case, which corresponds to an absolutely unstable flow[12]. A Cartesian grid of 601 by 281 is used with the the same grid spacing in both two directions, $\Delta x = \Delta y = 0.32\delta_\omega(0)$, where $\delta_\omega(0) = 0.0016$ m.

5.2.2 Inflow forcing

The counterflow mixing layer is (locally) absolutely unstable at any streamwise location, the wave packet spreads in both upstream and downstream directions. This would contaminate the upstream boundary, yielding spurious noise. Since the inflectional point of the velocity profile is responsible for the inviscid instability growth (the so-called Kelvin-Helmholtz instabilities), we try to make the mixing layer more spread by enlarging the base flow vorticity thickness to prevent the birth of wave packets near the boundaries. That is why only the strictly parallel domain from $x = -100\delta_\omega(0)$ to $x = 100\delta_\omega(0)$ in the streamwise direction is analyzed. The initial forcing is provided by a concentrated pulse of the form :

$$u'(x, y, t = 0) = A \exp\left(-\frac{(x - x_0)^2 + (y - y_0)^2}{\Delta y^2}\right) \quad (7)$$

with amplitude $A = 10^{-4}$ m/s located at the center (x_0, y_0) of the absolutely unstable region.

5.2.3 Near-field hydrodynamic results

Figure 5 shows snapshots of the total spanwise vorticity ω_{xy} at four successive instants. First pairings appear in both upstream and downstream directions as they are advected away from the source. Pairing process take place in a symmetric manner. At the upstream and downstream boundaries, no vortex structure is seen because of the widening of the base flow. The violent nature of the vortex ejection shows the limit of the two-dimensional approach. 3-D simulations seem valuable to allow the vortex stretching in the spanwise dimension.

5.2.4 Linear stability calculation

The diagram in figure 6 illustrates the propagation of the transverse velocity perturbation v' at the center of the domain as a function of time and streamwise location. The unstable wave packet is bounded in $(x, t)-$ plane by the trailing- and leading-edge rays $x/t = v^-$ and $x/t = v^+$, along which the temporal growth rate is zero. Disturbances grow exponentially and gradually contaminate the entire medium which is typically the characteristics of absolute instability mechanism.
The temporal growth rate is obtained by the classical pinching process of two distinct spatial $\alpha^+(L_\omega)$ and $\alpha^-(L_\omega)$ branches in the complex plane (α_r, α_i), along the ray $x/t = V = 0$, where V is the group velocity, and L_ω is the integration contour in the complex $\omega-$ plane.

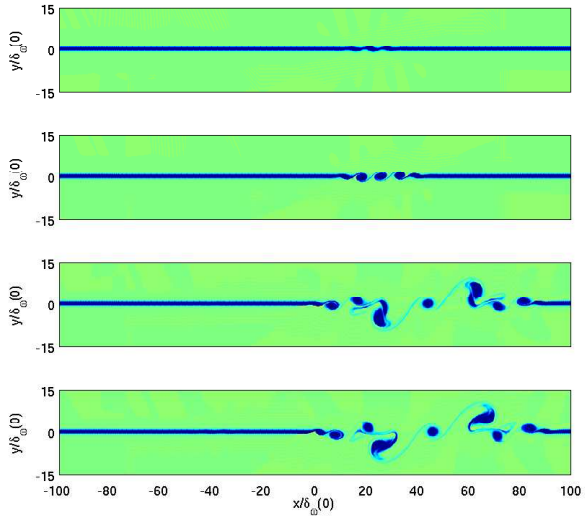

FIG. 5: Total vorticity field of the two-dimensional counterflow mixing layer at four instants. Levels from -5×10^4 to $5 \times 10^4 \mathrm{s}^{-1}$

This typical scenario is illustrated in figure 7. The absolute growth rate for $R = 1.67$ and $M_c = 0.29$ is found to be $\omega_{0,i} = 0.092$.

6 3-D simulation of a coflow mixing layer

Two-dimensional assumption is usually made to simplify the investigation of the plane mixing layer dynamics from a computational point of view. However, the overestimated transverse velocity fluctuation statistics and neglect of Reynolds stresses demand accounting for three-dimensionality.

6.1 Numerical parameters

A Cartesian grid of $600 \times 300 \times 51$ points in the x, y and z directions respectively, is used. The initial vorticity thickness is chosen to be $\delta_\omega(0) = 0.00512$ m. The grid is uniform in x with spacing $\Delta x = 0.4\delta_\omega(0)$ over the first 540 points. The grid is then streched over the last 60 points. The Laplacian filter constitutive of the sponge region is added over the last 70 points. In the transverse direction, the grid is stretched with a rate of 1.8%, with a minimum spacing of $\Delta y = 0.4\delta_\omega(0)$ inside the shear layer. The computional domain extends over $x = 70\delta_\omega(0)$ in the streamwise direction, from $y = -90\delta_\omega(0)$ up to $y = 90\delta_\omega(0)$ in the normal direction and from $z = -3\delta_\omega(0)$ to $z = 3\delta_\omega(0)$ in the spanwise direction. Periodic boundary conditions are applied in the spanwise direction. The CFL number is fixed at 0.9. The calculations have been performed in parallel using 8 processors of NEC-SX8.

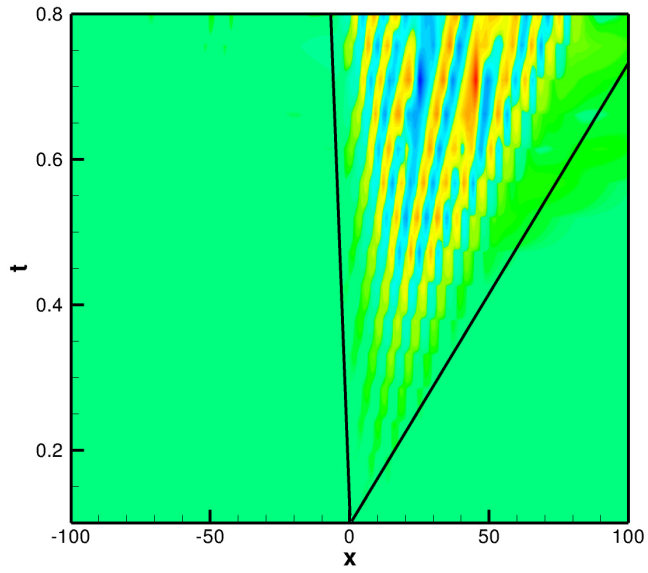

FIG. 6: Spatio-temporal evolution of v' at the center of the computional domain.

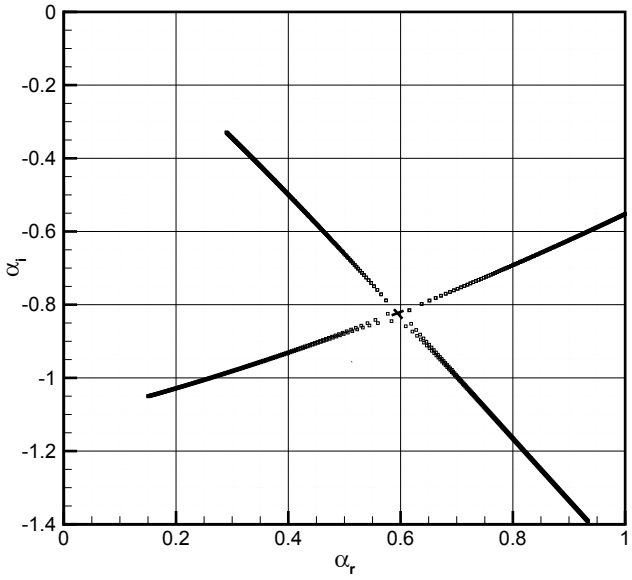

FIG. 7: Locus of spatial branches $\alpha^+(L_\omega)$ and $\alpha^-(L_\omega)$ as the L_ω contour is lowered in the complex $\omega-$ plane.

6.2 Inflow forcing

The same inflow forcing as used in the 2-D coflow case is replicated in the spanwise direction, *i.e.* it is based on a combination of f_0 and its subharmonic $f_0/2$ to fix the location of the first pairing. The amplitude in (6) are now $\alpha_1 = 4.10^{-4}$ and $\alpha_2 = 2.10^{-4}$ m/s. A small random noise with an amplitude of 5.10^{-5} m/s is added on the spanwise velocity component at the initial time to trigger the three-dimensionalities.

6.3 Near-field hydrodynamic results

The three-dimensional vortex structures are shown in figure 8 with the Q criterion [13]. As we can see, the mixing layer first evolves into primary, spanwise-organized, Kelvin-Helmholtz vortices, and then undergoes the first pairing. Intense longitudinal braids stretched between Kelvin-Helmholtz vortices are found, as oberved by Bernal & Roshko [14]. Further downstream, large vortices evolve into small-scales structures which is an obvious evidence of fully developed three-dimensional characteristics.

6.4 Acoustic radiation

The resulting acoustic far-field is visualized in figure 9 for the three-dimensional case, the dominant source is located near $x = 60\delta_\omega(0)$. As expected, a lateral quadrupolar source is identified in the acoustic near-field. Also, wavefronts emanate from the vortex pairing location, but seem to be less regular compared to the two-dimensional case, with several waves in the upper region. This can maybe be explained by the appearance of a three-dimensional modulation. Note that radiation levels are slightly weaker since the transition to turbulence during the pairings gives a less coherent event.

FIG. 8: Total vorticity field of the three-dimensional coflow mixing layer. View of an isosurface of the Q-criterion at the value 10^{-5} colored with the streamwise vorticity (levels between $\pm 10^5$ s^{-1}).

7 Concluding remarks

In this paper, the sound generated by coflow and counterflow mixing layers is investigated in order to link the noise radiation with the particular waves instability. A coflow shear layer is indeed prone to convective Kelvin-Helmholtz-type instabilities whereas a counterflow one induces a local absolute instability. The sound radiated from excited coflow mixing layers has been carried out using two- and three-dimensional simulations of the nonlinear disturbance equations. Results from DNC show that acoustic waves at the frequency $f_0/2$ emanate from the pairing location, which is fixed by a particular forcing. Though the computation of counterflow mixing layers are still two-dimensional, the oscillator behaviour of the absolutely unstable flow is clearly exhibited. Three-dimensional simulations are needed to explore the sound radiation associated with this kind of global instability.

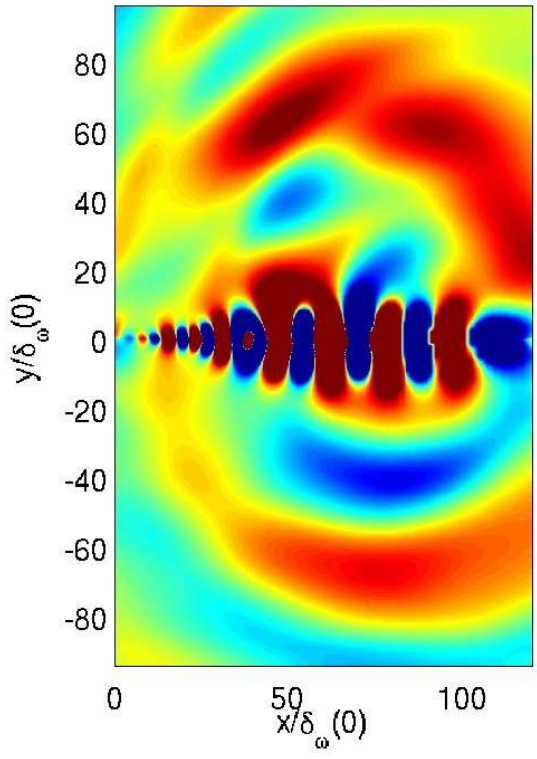

FIG. 9: Far-field pressure for the three-dimensional coflow mixing layer forced at f_0 and $f_0/2$. Pressure levels from -50 Pa to 50 Pa.

Acknowledgments

This work was granted access to the HPC resources of IDRIS and CCRT under the allocation 2009-41736 made by GENCI (Grand Equipement National de Calcul Intensif).

Références

[1] P. Comte, M. Lesieur and E. Lamballais, "Large and small-scale stirring of vorticity and a passive scalar in a 3D temporal mixing layer", *Phys. Fluids* A 4, 2761-2778 (1992)

[2] T. Colonius, SK. Lele and P. Moin, "Sound generation in a mixing layer", *Journal of Fluid Mechanics* 330 (1997)

[3] C. Bogey, C. Bailly and D. Juvé, "Numerical simulation of sound generated by vortex pairing in a mixing layer ", *AIAA Journal* 38(12),2210-2218 (2000)

[4] A. Babuke, M. Kloker and U. Rist, "DNS of a plane mixing layer for the investigation of sound generation mechanisms", *Computers & Fluids* 37, 360-368 (2008)

[5] C.K.W. Tam and P.J. Morris, "The radiation of sound by the instability waves of a compressible plane turbulent shear layer", *Journal of Fluid Mechanics* 98, 349-381 (1980)

[6] C.K.W. Tam and D. Burton, "Sound generation by instability waves of supersonic flows", Part 1. Two dimensional mixing layers. *Journal of Fluid Mechanics* 138, 249-271 (1984a)

[7] C.K.W. Tam and D. Burton, "Sound generation by instability waves of supersonic flows", Part 2. Axisymmetric jets. *Journal of Fluid Mechanics* 138, 273-295 (1984b)

[8] P.J. Morris, L.N. Long, A. Bangalore and Q. Wang, "A parallel three-dimensional computational aeroacoustics method using nonlinear disturbance equations", *Journal of Computational Physics* 133, 56-78 (1997).

[9] C.K.W. Tam and J.C. Webb, "Dispersion-Relation-Preserving Finite Difference Schemes for Computational Acoustics", *Journal of Computational Physics* 107(2), 262-281 (1993).

[10] C. Bogey and C. Bailly, "A family of low dispersive and low dissipative explicit schemes for flow and noise computations", *Journal of Computational Physics* 194, 194-214 (2004).

[11] C.K.W. Tam and Z. Dong, "Radiation and Outflow boundary conditions for direct computation of acoustic and flow disturbances in a nonuniform mean flow", *Journal of Computational Physics* 4(2), 175-201 (1996).

[12] P. Huerre and P. A. Monkewitz, "Absolute and convective instabilities in free shear layers", *Journal of Fluid Mechanics* 159, 151-168 (1985).

[13] J. Jeong and F. Hussian, "On the identification of a vortex", *Journal of Fluid Mechanics* 285, 69-74 (1995)

[14] L. P. Bernal and A. Roshko "Streamwise vortex structure in plane mixing layer", *Journal of Fluid Mechanics* 170, 499-525 (1986)